One pot environmental friendly synthesis of gold nanoparticles using Punica Granatum Juice: A novel antioxidant agent for future dermatological and cosmetic applications

One pot environmental friendly synthesis of Gold Nanoparticles using *Punica Granatum* Juice: a novel antioxidant agent for future dermatological and cosmetic applications.

*Jennifer Gubitosa,[a] Vito Rizzi,[b] Angela Lopedota,[a] Paola Fini,[c] Anna Laurenzana,[d] Gabriella Fibbi,[d] Fiorenza Fanelli,[e] Andrea Petrella,[f] Valentino Laquintana,[a] Nunzio Denora,[a] Roberto Comparelli,[c] Pinalysa Cosma[b,c]**

[a]Dipartimento di Farmacia-Scienze del Farmaco - Unità di Tecnologia farmaceutica, Università degli Studi di Bari "A. Moro", via Orabona 4, 70125 Bari, Italy;
[b]Università degli Studi "Aldo Moro" di Bari, Dip. Chimica, Via Orabona, 4 - 70126 Bari, Italy;
[c]Consiglio Nazionale delle Ricerche CNR-IPCF, UOS Bari, Via Orabona, 4 - 70126 Bari, Italy;
[d]Dipartimento di Scienze Biomediche Sperimentali e Cliniche "MarioSerio" Viale Morgagni 50 - 50134, Florence, Italy;
[e]Consiglio Nazionale delle Ricerche, Istituto di Nanotecnologia (CNR-NANOTEC) c/o Dipartimento di Chimica, Università degli Studi "Aldo Moro", Via Orabona, 4 - 70126 Bari, Italy.
[f]Dipartimento di Ingegneria Civile, Ambientale, Edile, del Territorio e di Chimica, Politecnico di Bari, Orabona, 4 - 70125, Bari, Italy.

Corresponding Author

*Pinalysa Cosma:
Università degli studi di Bari "Aldo Moro"
Dipartimento di Chimica, Via Orabona 4-70126 Bari, Italy
Tel: +390805443443
Fax: +390805442129
E-mail pinalysa.cosma@uniba.it

Abstract

Hypothesis: The interesting properties of Gold Nanoparticles (AuNPs) make them attractive for different application fields such as cosmetology, medicine and clinical nanotechnologies. In this work a fast, easy and eco-friendly method for the AuNPs synthesis is proposed by using the *Punica Granatum* Juice (PGJ) with potential dermatological and cosmetic applications. The AuNPs antioxidant activity, due to the presence of phenols from the juice, and their use as booster for improving the Sun Protection Factor (SPF) in commercial sunscreen formulations, are thus expounded.

Experiments: By using appropriate amounts of PGJ and $HAuCl_4$, under mild work conditions, AuNPs with a mean size of 100 ± 40 nm are observed and carefully characterized. Solution pH, temperature, and volume were also changed for optimizing the AuNPs formation and features. The antioxidant activity was studied, by evaluating the AuNP ability of scavenging the radical 2,2-diphenyl-1-picrylhydrazylhydrate (DPPH). This finding was confirmed performing special experiments focused on the reaction between AuNPs and H_2O_2, by using suitable probes, such as 4-thiothymidine (S^4TdR) and Cytochrome-c (Cyt-c). The SPF value was also calculated.

Findings: The synthetized AuNPs showed a surface plasmon in visible range at 577 nm and resulted stable for long time in aqueous medium, also changing the pH values in the range 2-12. The studied antioxidant activity, confirmed also by performing special experiments with suitable probes, demonstrated the high performance of AuNPs. The AuNP photostability under sun irradiation is also shown. The calculated SPF values were in the range 3-18, related to AuNPs concentration in the range 1.80×10^{-12} M - 1.00×10^{-11} M. The same AuNPs concentrations were used for cellular experiments. Indeed, since the AuNPs-PGJ mediated will be potentially introduced by dermal contact, dermal fibroblasts (Human Dermal Fibroblasts, HDF) and Human Microvascular Endothelial Cells (HMVEC) were used to evaluate the possible effects of these nanoparticles as a preliminary step. The results indicated that an AuNP

concentrations in the range 1.80×10^{-12} M - 3.60×10^{-12} M could be adopted since they do not appeared cyctotoxic.

Keywords: Gold Nanoparticles, sunscreens, antioxidants, Punica Granatum Juice, green synthesis, nanomaterials.

1. Introduction

Since ancient times, the medicinal properties and health beneficial effects attributed to bioactive compounds in fruits are object of study.[1] Interestingly, among fruits, the pomegranate (PG, *Punica granatum L.*) is considered exceptional, having noticeable properties. Despite these fruits were studied for years,[1] the development of PG-based more complex systems is still object of study. The high antioxidant *Punica Granatum* Juice (PGJ) activity was recently presented by Kalaycıoglu *et al.*[2], with interesting information also in the older work of Noda *et al.*[3], where authors reported the antioxidant activities of pomegranate fruit extract, focusing their attention towards the antioxidant properties of anthocyanidins as delphinidin, cyanidin, and pelargonidin, as H_2O_2 scavengers.[3] The PGJ main components efficiently act against several diseases (such as tumors, type 2 diabetes, atherosclerosis and so on),[4] showing also antimicrobial, anti-hepatoxic and antiviral properties, attributable to their high antioxidant capacity.[5,6] Focusing the attention on juice specific components, the work of Yoshimura *et al.*[7] showed the noteworthy property concerning the ellagic acid inhibitory effect on the tyrosinase activity, reducing the ultraviolet-induced pigmentation.[7] Again, more recently, in the C.L. Marchiori *et al.*[8] work, the juice main components were considered as potential sunscreens, evidencing the actual and novel interest towards the PGJ against skin ageing. As well described by Mbanga *et al.*,[9] a premature skin ageing is a direct consequence of the sunlight/skin interaction, inducing also malignant melanoma particularly due to the UV light exposure. Consequently, the high absorption of the PGJ-components in the UV region, screening the UVA and UVB radiations, could reduce the sun dangerous effect.[9-12] Indeed, recently, Xian *et al.*[13] evidenced as the skin photodamage was associated with the Reactive Oxygen Species (ROS) UV-induced production and the inactivation of NF-E2-related factor 2 (Nrf2): the excessive ROS production by UV high dose inactivates Nrf2, affecting the

Nrf2/antioxidant response pathway, reducing the antioxidant defense system, so that some cutaneous disorders are observed.[13]

The PGJ potential is so great and the list of its properties is so wide, that it is difficult to exhaustively describe the enormous number of its applications. In the present work, the attention was focused towards the juice antioxidant activity, its ability in screening the sun radiation and reducing metals, forming nanostructure. To the best of our knowledge, this study shows the ecofriendly formation of PGJ-induced AuNPs, as novel efficient platform combining the PGJ antioxidant and sunscreen properties with AuNP biomedical properties. Generally, AuNPs could be efficiently prepared using a lot of different methods and applications,[14] most of which involve chemical compounds, toxic for the environment and human health.[15] Thus, plant-based synthesis of AuNPs is gaining importance due to its low cost, high reproducibility and eco-friendliness.[15] Abdelmonema *et al.*[16] reported as the bio-inspired techniques easily offer the fabrication of nanostructures, uniform in size and shape, providing more biocompatible nanoparticles than chemical synthesis. Indeed, the latter may lead to the presence of some toxic chemical species on the nanoparticle surface, undesirable for biomedical applications.[16] In this work, the PGJ, used without further purification, easily forms uniform AuNPs. The phenols involved in the AuNP formation reaction,[15] not only scavenge the oxidative species, but, coating the nanoparticle surface, are also able to screen the sun radiations. The antioxidant properties of capped AuNPs, obtained with different methods, have been known for years,[17-19] however interesting applications are described in the recent work of Jiménez-Pérez *et al.*[20] The authors reported the AuNPs Panax ginseng leaves-mediated synthesis showing the antioxidant properties, moisture retention, and whitening effects of the AuNPs proposing them in cosmetic formulations.[20] Borase *et al.*[21] explored the phytolatex synthesized AuNPs as novel agent to enhance the sun protection factor of commercial sunscreens, reporting as, in 1999, the Food and Drugs Administration allowed the use of

nanoparticles in commercial preparations. The authors suggested that the obtained AuNPs could be potentially used as SPF enhancement agents in sunscreens formulations, as alternative to the traditional nanostructured TiO_2 and ZnO, that suffered from side effects such as irritation, percutaneous absorption, photomutagenicity and immunoreaction.[21]

AuNPs appear more advantageous in cosmetic formulations due to their light absorption and scattering ability, biocompatible nature, low toxicity.[21] If these positive aspects are associated with the use of an eco-friendly protocol for their synthesis, a great interesting space is opened toward the study of antioxidant PGJ-based AuNPs for enhancing the SPF in sunscreen formulations. The AuNP antioxidant capacity was evaluated using the DPPH assay.[22] While, H_2O_2, an oxidant agent found in high level during the skin photodamage,[23] was used in presence of model biomolecules (S^4TdR and Cyt-c), for studying the AuNP ability in preventing biomolecule degradation, under strong oxidative conditions. S^4TdR is an analogue of thymidine (TdR), with the oxygen atom in position 4 replaced by a sulphur atom, obtaining a nucleoside with a marked reactivity towards ROS.[24-26] While, Cyt-c, being involved in several biological functions,[27] was used as a model protein for showing as AuNPs are able to prevent the oxidative protein degradation. Finally, for calculating the SPF, the guidelines reported by Mbanga *et al.*[9] and Dutra *et al.*[11] were adopted. Further, the PGJ-mediated AuNP stability under sun irradiation, together with the thermo- and time stability were also evaluated. Finally, nanotoxicological studies are also presented. The vast majority of trials concerning AuNP-toxicity are performed using somatic cell culture lines,[28] generally focusing on short term effects (less than 24h)[29-32] of particle exposure, instead of more long term treatment that can interfere with the proper execution of specific cellular function. Notably, for improving the experimental conditions of nanoparticle toxicity studies, the cell type should be selected taking into account the administration route and target organ of the nanoparticle. Since PGJ-mediated AuNPs will be introduced by the dermal contact, we selected dermal fibroblasts (Human

Dermal Fibroblasts, HDF) to evaluate the possible detrimental effects of these nanoparticles. Further, extensive studies have been done using endothelial cells (Human Microvascular Endothelial Cells, HMVEC) as a relevant model, since they lining the lumen of all blood vessels they serve as first contact with NPs.[33,34] We show that the HDF and HMVEC viability is not affected by long term exposure of PGJ-mediated AuNPs in the following concentration range 1.80×10^{-12} - 3.60×10^{-12}M. Safe and feasible antioxidant AuNPs for possible sunscreen formulations with a an SPF value of 6 are presented. Moreover, we observe that HMVEC enrichment with AuNPs does not interfere with the cell capability of forming a network of tube-like structures and eventually lumen-containing vessels. The interesting PGJ phenol antioxidant function and the important role in clinical treatment are thus presented in this study, proposing a good starting point to develop novel antioxidants with improved properties.[35]

2. Material and Methods

2.1. Chemicals.

$HAuCl_4$ was purchased from Sigma-Aldrich (Milan, Italy). The same commercial source was adopted for KH_2PO_4 and KOH, used to prepare buffer solutions at pH 7/pH 12, for KCl used for Zeta potential measurements, for DPPH and Cytochrome–c from equine heart (purity 95+% and used as received). *Punica Granatum* fruits were obtained from a local garden in Bari, south of Italy. 4-thio(2'-deoxy)thymidine (S^4TdR), having 99+% purity, was purchased from Carbosynth (Compton, Berkshire, UK) and used as received.

2.2 *Punica Granatum* Juice preparation. Fruits were transported to our laboratory at University of Bari (south of Italy), Dipartimento di Chimica and Dipartimento di Farmacia-Scienze del Farmaco-Unità di Tecnologia Farmaceutica. The fruits that appeared damaged were removed and those with uniform size and appearance were well washed for juice extraction. The fruits were cut in two halves and the juice was extracted using a glass squeezer. In order to

remove undesired peel and seeds, the obtained juice was centrifuged using a Thermo Scientific Heraemus Multifugue X3R Centrifuge. Subsequently the juice was immediately stored at -20°C in the dark. UV-Vis spectroscopy analyses were used to assess the stability of the juice during the work.

2.3 Experimental procedures. $HAuCl_4$ was dissolved in deionized water to obtain 2.0×10^{-4} M, 1.0×10^{-3} M and 1.0×10^{-2} M stock solutions. Appropriate amounts of these solutions were mixed with the PGJ and/or water obtaining different $HAuCl_4$ concentrations (see **Table 1** for more details). The role of the pH values during the synthesis was also evaluated using buffer solutions at pH 7 or 12. It is worth to mention that the pH of the juice was around 3; so when not directly indicated the AuNPs synthesis was performed at the pH of the PGJ. The mixtures were moderately stirred for 24h at room temperature. In detail, the UV–Vis spectroscopy analyses of these solutions were carried out soon after the preparation, and after 1, 4, 6 and 24 h. These samples were washed with fresh water before the analysis (dilutions were also performed, if necessary). The typical surface resonance plasmon exhibited by AuNPs was diagnostic to determine the presence of the nanostructured gold. For each time of analysis, the samples were purified removing the juice excess and the unreacted $HAuCl_4$ using a centrifuge (7000 g, for 10 minutes). The pellets were washed with fresh water for three time, until neutral pH was obtained, and properly diluted before the spectra acquisition. Experiments were also performed changing the temperature of solution containing the outcoming AuNPs. A heating magnetic stirrer (Arex, Velp Scientifica) equipped with a MGW Lauda R42/2 digital thermometer was used to change and control the temperature values.

2.4 UV-Visible measurements. Visible absorption spectra were recorded using a Varian CARY 5 UV-Vis-NIR spectrophotometer (Varian Inc., now Agilent Technologies Inc., Santa Clara, CA, USA) in the range 200-800 nm. Measurements were performed using a cuvette with a 1 cm and/or 0.1 cm path length.

2.5 Scanning Electron Microscopy (SEM). In the case of SEM analysis, an electron microscope FESEM-EDX Carl Zeiss Sigma 300 VP was used. The samples were fixed on aluminum stubs and then sputtered with graphite by the use of a Sputter Quorum Q150. Additionally, the chemical composition of AuNPs was determined by EDX under the scanning electron microscope and X-rays diffraction.

2.6 X-ray Photoelectron Spectroscopy (XPS) and FTIR spectroscopic measurements. The infrared absorption spectrum of the AuNPs was acquired in transmission mode in the range 375–4000 cm^{-1} with a resolution of 4 cm^{-1} using a vacuum Bruker Vertex 70v Fourier transform infrared (FTIR) spectrometer. X-ray photoelectron spectroscopy (XPS) analyses were performed using a PHI VersaProbe II spectrometer equipped with a monochromatic Al Kα X-ray source (1486.6 eV) operated at a spot size of 200 μm, corresponding to a power of 47.2 W. Survey (0−1400 eV) and high resolution (C 1s, O 1s, N 1s, Au 4f) spectra were recorded in FAT (fixed analyzer transmission) mode at pass energy of 117.4 eV and 46.95 eV, respectively. All spectra were acquired at a take-off angle of 45° with respect to the sample normal. Dual-beam charge neutralization was constantly applied during analysis. Charge correction of the spectra was performed by taking the hydrocarbon component of the C 1s spectrum as internal reference (binding energy, BE=284.7 eV). Detailed spectra processing was performed by commercial MultiPak software (Version 9.5.0.8, 30-10-2013, Ulvac-PHI, Inc.). The high-resolution spectra were fitted with mixed Gaussian-Lorentzian peaks after a Shirley background subtraction. A maximum relative standard deviation of 10 % was estimated on the area percentages of the curve-fitting components, while the determined standard deviation in their position was ±0.2 eV. For both XPS and FTIR analyses the nanoparticles were dispersed in ethanol, deposited by drop-casting onto small pieces of a Si(100) wafer, and analyzed after solvent evaporation at room temperature.

2.7 Transmission electron microscopy (TEM). The analysis was performed by a JEOL JEM-1011 microscope operating at 100 kV. The TEM samples were prepared by casting a drop of AuNPs aqueous solution onto a carbon coated copper TEM grid (400 mesh) and letting the solvent to dry at room temperature. At least 100 NPs have been counted for statistical analysis.

2.8 Zeta potential and size measurements. The average of the hydrodynamic diameters and the polydispersity index (PDI) of the NPs were measured by dynamic light scattering and using a Zetasizer Nano ZS (Malvern Instruments Ltd., Worcestershire, UK) after suitable dilution of bulk suspensions in demineralized water. The surface charge of NPs was measured as zeta potential by laser doppler velocimetry using the same instrument after dilution with 1 mM KCl.

2.9 Photostability, thermostability and temporal stability of AuNPs. The AuNPs photostability was evaluated by irradiation with a sun simulator lamp purchased from Oriel Corporation, Stratford. Conn, USA, Model 6684. A Xenon lamp (150 W) with a E_0: 1482 mW/cm^2~1.48 suns was used. The solution containing AuNPs was placed at 6.5 cm from the source located at 18.5 cm from the growth. AuNPs aqueous solution was irradiated for 90 minutes and UV-Vis spectra were acquired each 30 minutes. Thermostability experiments were performed using a heating magnetic stirrer (Arex, Velp Scientifica) using MGW Lauda R42/2 digital thermometer. Temporal stability measurements were performed monitoring the UV-Vis spectrum of AuNPs at different storage time. Experiments were undertaken in aqueous solutions to mimic the conditions actually occurring in physiological systems.

2.10 Determination of the Sun Protection Factor. Dutra *et al.*[11] and Mbanga *et al.*[9], present a very simple mathematical equation utilizing UV spectrophotometry to determine the SPF in the UVB region. In particular Borase *et al.*[21] apply **Equation 1** for the calculation of SPF:

$$\mathbf{SPF}_{Spectrophotometric} = \boldsymbol{CF} \times \sum_{290}^{320} \boldsymbol{EE}\,(\boldsymbol{\lambda}) \times \boldsymbol{I}\,(\boldsymbol{\lambda}) \times \boldsymbol{Abs}\,(\boldsymbol{\lambda}) \qquad \textbf{Equation 1}$$

Where: EE (λ) is the erythemal effect spectrum; I (λ), the solar intensity spectrum; Abs (λ) is the absorbance of standard solutions of the sunscreen product in the wavelength region 290-320 nm; CF, the correction factor (=10). The values of EE (λ) × I (λ) are constants and were determined by using the procedure and the Table reported in references 9 and 11.

2.11 Determination of DPPH radical scavenging capacity. The antioxidant capacity of AuNPs was evaluated using as probe the 2,2-diphenyl-1-picrylhydrazylhydrate (DPPH).[22] Four different AuNP concentrations, ranging between 0.6×10^{-12} M and 3.6×10^{-12} M, were adopted in presence of DPPH radical 8.3×10^{-4} M. Methanol was used as solvent. After leaving for 30 minutes in the dark at room temperature, the absorbance spectra of DPPH were recorded monitoring the absorption band at 517 nm.[22] The total antioxidant activity was calculated as percentage of DPPH discoloration using **Equation 2**.

$$\%\ \textbf{Antioxidant Activity} = \frac{\mathbf{A_{DPPH} - A_{sample}}}{\mathbf{A_{DPPH}}} \times 100 \qquad \textbf{Equation 2}$$

where, A_{Sample} is the absorbance value at 517 nm, of the solution containing AuNPs and DPPH after 30 minutes and A_{DPPH} is the absorbance value of the DPPH solution before the addition of AuNPs. Results were expressed as amount of AuNPs required to scavenge the 10 % of DPPH radicals. The same experiment was performed using 6-hydroxy-2,5,7,8-tetramethylchroman-2-carboxylic acid (TROLOX) as a positive control.[22] The TROLOX concentrations ranging from 1.0×10^{-6} M to 1.0×10^{-4} M were adopted.

2.12 Antioxidant ability of AuNPs against H_2O_2. To test the antioxidant ability of AuNPs against H_2O_2, different methods were adopted. S^4TdR and Cyt–c were used as suitable probes to detect H_2O_2 in presence and in absence of AuNPs. Using the UV-Vis spectroscopy, the probe degradation was used to infer information about the AuNP antioxidant activity scavenging H_2O_2.[54,55] A stock solution of Cyt–c, with a 5 mg/mL concentration, was diluted to obtain Cyt–c solution with a final concentration of 0.1 mg/mL. AuNPs at concentrations of 1.80×10^{-12} M, 3.60×10^{-12} M, 7.20×10^{-12} M and 1.00×10^{-11}M were added in the solutions. The protein

degradation was monitored following the time evolution of the visible spectrum at 408 nm and 535 nm in water medium.[54,55]

The percentage of Cyt–c degradation at different time (*t*) was calculated using the following Equation:

$$\textbf{\% DEG (Cyt}-\textbf{c)} = \frac{[Cyt-c]_0-[Cyt-c]_t}{[Cyt-c]_0} \times 100 \qquad \textbf{Equation 3}$$

where $[Cyt–c]_0$ is the concentration of Cyt–c before the addition of H_2O_2 and $[Cyt–c]_t$ the concentration at time *t*. A S^4TdR stock aqueous solution 5.0×10^{-3} M was properly diluted obtaining a solution 1.0×10^{-3} M. The AuNP concentration in this case was settled at 3.60×10^{-12} M and 1.00×10^{-11} M. The nucleoside degradation was monitored through its UV-Vis spectrum, following the main absorption band at 337 nm in water medium.[24,25,26] For S^4TdR, a cuvette having 0.1 cm path length was used. Experiments were undertaken in aqueous solutions to mimic the conditions actually occurring in physiological systems.[24,25]

2.13 Cell cultures. Human microvascular endothelial cells H-MVEC (Lonza, Basel, Switzerland) were maintained in complete endothelial cell growth medium (EGM-2 Bullet Kit), which includes endothelial basal medium (EBM-2) plus the Single Quots Kit (hydrocortisone, human fibroblast growth factor B, VEGF, LongR3 insulin-like growth factor 1, ascorbic acid, human epidermal growth factor, GA-1000, and heparin) (Lonza, Basel, Switzerland). HMVECs were used between the third and seventh passages in culture. Human Dermal Fibroblasts (HDF) (Sigma-Aldrich, Darmstadt, Germany) were maintained in DMEM medium supplemented with 10% fetal calf serum (FCS). Fibroblasts were used between the third and 15th passages in culture

2.14 Cell viability determination. The viability of HMVECs and HDF was determined by trypan blue staining. Cells (1.0×10^5) were seeded in 6-well plates and allowed to attach overnight. On the next day AuNP colloidal solutions were added at the indicated concentrations. 72 h later 20 µl of cells were aseptically transferred to a 1.5 mL clear Eppendorf tube and

incubated for 3 min at room temperature with an equal volume of 0.4 % (w/v) trypan blue solution prepared in 0.81 % NaCl and 0.06 % (w/v) dibasic potassium phosphate. Viable and nonviable cells (trypan blue positive) were counted separately using a dual-chamber hemocytometer and a light microscope. The means of three independent cell counts were pooled for analysis.

2.15 Capillary morphogenesis. Matrigel (0.05 mL; 9 – 11 mg/mL) was pipetted into 96 well tissue culture plates and polymerized for 30 min to 1h at 37 °C as previously described.[58] Cultures were pre-treated with/without AuNPs at the indicated concentrations for 24 h and then aliquots of HMVEC (2×10^4) were plated in EBM-2 medium, supplemented with 2 % FCS and incubated at 37 °C - 5 % CO_2. Morphogenesis was evaluated taking pictures after 6h with the aid of a Nikon E 4500 photocamera (Nikon) on a Nikon TMS-F phase-contrast microscope (Nikon Instruments). Six to nine photographic fields from three plates were scanned for each point. Results were quantified by measuring the number of closed meshes expressed as percent ± SD in respect to control set as 100 %. Meshes were identified as the empty region of the field delimited by tubules and cell clusters.

2.16 Optical microscopic analysis. Morphological features of cells treated with AuNPs were microscopically examined using a Digital Camera System Leica DC 200 (Leica Microsystems, Inc. Bannockburn, IL, USA). Cells were seeded on 6-well plates at a density of 1.0×10^5. The next day, the medium was replaced with fresh medium containing dilutions of AuNPs at concentrations 1.80×10^{-12} M, 3.60×10^{-12} M, 1.00×10^{-11} M. After 72h of incubation (37 °C, 5 % CO_2), the medium was removed and the cells were stained with May-Grunwald Giemsa. Briefly, 1mL of May-Grünwald stain was added per well and after 7 min, it was diluted with an equal amount of distilled water. After 2 min, the stain was replaced with 1mL of Giemsa stain (diluted 1:20 in distilled water). After 7 min, the stain was removed and the cells were washed thoroughly with distilled water.

3. Results and Discussion

3.1. Overview

It was observed that, by adding PGJ to aqueous solutions containing appropriate $HAuCl_4$ amounts, the color of the reaction mixture changed from pale yellow to red in a reasonable time range. Elapsing the contact time, the color of these solutions changed gradually to dark red. In particular, the first change in color was observed after 5 minutes from the PGJ addition, but the typical reddish color of nanostructured Au solutions appeared after 20 minutes, without further modification in elapsing time. This chromatic evolution (from A, containing only $HAuCl_4$, to F, after 20 minutes from the juice addition) is shown in the camera pictures in **Figure 1(A-F)**, referred to the experiment in the best condition and producing AuNPs 100 ± 40n m wide.

3.2. Synthesis and characterization of AuNPs.

The preliminary step of this study was based on the UV-Vis investigation of aqueous solutions containing $HAuCl_4$ and appropriate amounts of PGJ. In these solutions, the AuNP presence was confirmed by observing the characteristic surface plasmon resonance (SPR) signal in the visible absorption spectrum.[15] The total volume and the $HAuCl_4$ concentration were carefully varied according the conditions reported in **Table 1**. Among all experimented reaction conditions, samples 1 and 2 didn't show the typical AuNP SPR band in UV-Vis spectra, suggesting the key role played by both $HAuCl_4$ concentration and added PGJ amount, in affecting the nanoparticle formation. The gold salt concentration were settled at 5.0×10^{-4} M, 2.5×10^{-4} M, 2.0×10^{-4} M, 1.50×10^{-4} M and 1.0×10^{-4} M and in all of adopted concentration the formation of AuNPs was not observed. In particular, sample 2 was indicative of how a PGJ excess was not helpful for the AuNPs formation. Moreover, for both samples, also changing the solution pH values (during the synthesis) and total volume, the results were not improved. On the other hand, the samples

labelled with number 3 appeared more interesting. More specifically, the samples from 3A to 3C differ for the final $HAuCl_4$ concentration, having been variously diluted with water and/or buffer solutions at pH 7 and/or 12, respectively. In these samples, a fixed PGJ volume of 500 μL was used. The UV-Vis spectrum of sample 3B1 is reported in **Figure 2A**. After 4h of stirring, the SPR band of AuNPs was observed at 577 nm. The same result was observed for sample 3A, indicating that the solution dilution unaffected the AuNP formation. In excellent agreement with literature,[15] the symmetric and well defined resonant plasmon suggested the presence of monodisperse and not aggregate AuNPs with a diameter in the range 50-150 nm, as further confirmed by observing the corresponding SEM image reported in Figure 2B. Indeed, AuNPs having a mean size of 100 ± 40 nm with irregular domains were observed, together with some aggregates. It is worth to mention that ultrasounds can replace the use of the stirrer enhancing the AuNPs formation. Indeed the time necessary to obtain the AuNPs can be reduced from 4h to 15 minutes under these conditions of work.

In order to confirm the chemical nature of AuNPs, the EDX analysis was performed (**Figure 3**), focusing on aggregated AuNPs in order to better evidence the obtained results. During the image acquisition for EDX analysis, the presence and nature of AuNPs were positively confirmed (see Figure 3A corresponding to the In-Lens SEM image). The white rectangle, around the bright field regions observed in Figure 3A, showed an high percentage of Au (52.00 ± 0.10 %). Besides, as depicted in Figure 3B, Au labelled with green color occurred uniformly and definitely distributed in the region in which AuNPs were observed.

Finally, maintaining the same experimental conditions, if the solution pH, during the synthesis, was changed from pH 3 to 7 and 12 (samples 3B2 and 3B3, respectively), aggregated and amorphous AuNPs with irregular domains were obtained, confirmed by a broader SPR signal (**Figure S1**), indicative of the sample polydispersity. Last but not least, **Table 1** reports the sample 3C, which differs from samples 3A and 3B1 only for the amount of the water added in

the final mixture. **Figures S2A** and **S2B** report the UV-Vis spectra (acquired at different contact time) and the corresponding SEM images, in which irregular particles were observed. The results indicated that the dilution with water, changing the final volume from 2 mL to 4 mL, favor the AuNP formation. In samples 4, in order to evaluate the effect of changing the ratio V_{Au}/V_E, the PGJ volume was halved, while the final Au^{III} concentration was increased, also varying the total water amount and final pH according to the scheme of samples 3. The measures, once again, indicated as the changes in the experimental conditions didn't significantly affect the AuNPs formation. For example, in Figures S2C-F, the more interesting results, related to 4C and 4D1 samples are reported. In these conditions, a mixture of gold nanorods and nanoparticles were observed. Further modification of the experimental parameters were performed (from sample 5 to sample 8 in Table 1), without obtaining any improvement of AuNP synthesis. It is worth to mention that experiments were also carried out increasing the solution temperature, finding that hot water didn't favor the AuNPs formation, but rather their aggregation.

Therefore, after this thorough investigation, among all explored conditions, the sample 3B1 appeared as the best one and it was carefully studied, excluding extreme conditions of reaction and using a simpler and faster method for producing AuNPs at room temperature without additional stabilizing agents. It is worth to mention that uniform AuNPs were obtained if compared with similar synthesis. [15]

For the obtained AuNPs, a molar absorption coefficient of $1.6 \times 10^{11}\ M^{-1}cm^{-1}$ was used, after observing as the Lambert-Beer law was respected. In fact, by reporting the maximum absorbance value at 577 nm against different AuNPs concentrations, a linear relationship was obtained (**Figure S3**). By adopting this molar absorption coefficient, each synthesis performed using the 3B1 condition (Table 1**)** produced AuNPs solutions at a concentration of 2.0×10^{-11} M.

3.3. Time evolution of the outcoming AuNPs.

As mentioned before, the AuNPs formation was followed by recording the UV-Vis spectra of the AuNP reaction mixture characterized by a SPR signal at about 577 nm. The absorption spectra were acquired after 1, 4, 6 and 24 h and the wavelength shift of the maximum absorption together with the Full-Width at Half-Maximum (FWHM) were used as diagnostic parameters of nanoparticle aggregation (**Figure S4**).[36] More specifically, in Figure S4, the $\Delta\lambda$s referred to 575 nm (the wavelength of the maximum absorbance observed after 1h of contact time) are reported as function of reaction time. Since wavelength shift towards higher values is indicative of nanoparticle aggregation,[36] the observed unimportant time changes suggested that the synthesis was very fast with the AuNPs formation occurred in the first hour after the PGJ addition, without a significative aggregation. This finding was confirmed also by the FWHM values,[37] which resulted quite uniformly distributed as function of the contact time (Figure S4). Therefore, 4h was chosen as the optimal contact time, indicating these experimental conditions of great practical value for a large-scale preparation of AuNPs. The obtained particles result stable for long time in water solution with a Zeta potential value of about -22 ± 2 mV.

3.4. FTIR spectroscopic measurements.

In agreement with literature,[15] under our experimental condition, the reduction of gold takes place in water under mild reaction conditions and the PGJ extract acts both as reducing as well as stabilizing agent. Since the PGJ contains different classes of polyphenolic compounds, Dash *et al.*[15] suggested that the reaction mechanism involves adjacent hydroxyl groups forming a five membered chelate ring, oxidable to the corresponding benzoquinones by either air or metal

ions, so Au^{III} is reduced to Au^{0}. The subsequent AuNP formation is favored by the formation of a stabilizing phenols-based organic layer on the gold surface.

In our case, the presence of the main components of the juice around AuNPs was confirmed observing both the UV-Vis (Figure 2A) and FTIR (**Figure S5**) spectra of AuNPs. Comparing **Figure S6,** showing the PGJ UV-Vis spectra at different dilutions, with Figure 2A**,** one can observe that the characteristic absorption signals of PGJ compounds at wavelength less than 400nm, are present also in the solution containing AuNPs. The observed bands were attributed to phenols and anthocyanins presents in the PGJ.[38-41] The AuNP FTIR spectrum showed a peak at 3296 cm^{-1} attributed to the –OH phenolic functionality (Figure S5). The signals at 2919 cm^{-1} and 2849 cm^{-1} were attributed to C–H stretching vibration. The band at 1655 cm^{-1} and a shoulder located around 1736 cm^{-1} indicated the presence of carboxyl groups in phenolic chemical structures. Also amine moieties were evidenced by the signal at 1534 cm^{-1}, suggesting the slight contribute of aminoacids.[41,42] Other bands below 1500 cm^{-1} were attributed to C=C of aromatic ring, C-O group stretching in ester and ether moieties, and C-N stretching of aliphatic primary amines.[15,43]

3.5. X-ray Photoelectron Spectroscopy (XPS) measurements.

In order to draw more detailed information about the AuNP generation, and to gain insights into the surface chemical composition of AuNPs prepared in this work, XPS analyses were carried out.

The results showed that the surface atomic concentrations of carbon, oxygen, nitrogen and gold are about 74, 22.5, 3 and 0.5 %, respectively. **Figure S7A** showed the high-resolution Au4f XPS spectrum consisting of a doublet (Au $4f_{7/2}$ and Au $4f_{5/2}$, respectively, at 83.7 and 87.4 eV) due to spin−orbit coupling, the position being in agreement with previous literature on AuNPs.[44-48] The curve fitting of the Au4f signal indicated two $Au4f_{7/2}$ components, *i.e.* the

main component at 83.7 eV (88 %) attributed to metallic gold (Au(0)) and the minor peak at about 84.8 eV (12%) ascribed to Au(I) (the total area of the Au $4f_{7/2}$ signal was taken as 100%).[46,48] The high-resolution C1s XPS spectrum in Figure S7B was curve-fitted with four peaks and, specifically, the hydrocarbon component at 284.7 eV (66 %), the component at 286.2 eV (24.5 %) ascribed to both C-O and C-N groups, the peak at 288.8 eV (8 %) assigned to both C=O and O-C-O moieties and the weak peak at 289.1 eV (1.5 %) indicative of carboxylic functionalities. The O1s spectrum in Figure S7C showed the main peak at 532.7 eV (82 %) that can be ascribed to O-C groups and the minor component at 531.1 eV (18 %) associated to O=C. The N1s signal (Figure S7D) presents one main peak at about 399.8 eV, consistent with the presence of amino groups.

3.6. Transmission electron microscopy (TEM).

The discussed hypotheses were further confirmed through the use of the TEM analysis. **Figure 4** shows the AuNPs morphological feature after several washing. A thin organic coating (approximately 6nm wide), evidenced by the light grey layer surrounding each NP, can be observed for all detected AuNPs. Moreover, AuNPs mainly show an irregular shape.

Temporal, thermal and pH dependence evolution of synthesized AuNPs. The AuNP stability under several different work conditions was evaluated. AuNPs were studied by changing the pH values of aqueous solutions (ranging from 2 to 12) and the temperature values (from 25 °C to 60 °C), by exposing the AuNP solution to sun irradiation, and by testing their time stability. **Figure 5A** reports the pH effect both on the AuNP SPR position in the UV-Vis spectra and on the related FWHM values. The results indicated that both the position and the FWHM were stable. Size and Zeta potential measurements reported in Figure 5B, confirmed these results with the exception of pH 2. Indeed, at this pH, a positive Zeta potential value, of approximately +4mV, and AuNPs with a size of around 400 nm were measured, with a PDI value of 0.320,

which indicates that the sample occurred slightly not homogeneous in the size distribution. The presence of dimeric AuNPs was thus supposed. On the other hand, up to pH 2, negative charged AuNPs with a mean size of 148 ± 12nm were observed. In detail, the AuNP diameters ranged from 136 nm to 160 nm, with PDI values included between 0.247 and 0.134, indicating quite monodisperse synthetized AuNPs, with experimental Zeta potential values in the range -18 to -26 mV (from pH 4 to 12, respectively). The Zeta potential is indicative of the AuNP suspension stability, since a higher electric surface charge (positive or negative) of the AuNPs prevents aggregation.[49] The presence of the discussed functional groups on the AuNP surface, produced a negative electrical charge and its dependence on the pH. At pH values below 2, the organic moieties are in the protonated form and the AuNPs aggregated due to the modification of the Zeta potential values. The measured high negative potential suggested the stability of AuNPs in water. Regarding the temperature effect, the SPR signal resulted to be stable at the increasing of temperature from 25 to 60 °C, with constant wavelength position and FWHM values (*data not shown*).

3.7. AuNPs stability under sun simulator lamp and calculation of the SPF.

Starting from the work of Borase *et al*.,[21] the AuNPs ability to screen the sun radiation thanks to the phenolic organic layer present on their surface was investigated. As first step, the AuNPs photostability was evaluated irradiating the solutions with a sun simulator lamp. **Figure S8** shows as the SPR band in the UV-Vis spectra was stable in both wavelength position and FWHM values, indicating that the system is photostable.

In general, to be effective in preventing sunburn and other skin damage, a sunscreen product should have a wide range of absorbance between 290 and 400 nm. Thanks to phenolic moieties present in the juice and used to induce the AuNPs formation, the AuNPs exhibited strong

absorption in this region, suggesting the possibility to use them as additional ingredient in sunscreen formulations.

For evaluating the effectiveness of sunscreen preparations to protect skin from harmful UV radiations, the universal SPF should be calculated. The SPF definition reported by Borase *et al*.[21] is the following: *"SPF is defined as time required for producing minimal perceptible erythema of sunscreen protected skin relative to time required for same damage to occur in unprotected skin".*[21] The *in vitro* methods for determining the SPF are in general of two types:[50] methods involving the measurement of UV radiation absorption or transmission of sunscreen product films between quartz plates or biomembranes, and methods determining the absorption characteristics of the sunscreen substances by means of spectrophotometric analysis of dilute solutions. The simple method applied in this work makes use of absorption spectroscopy experiments followed by the **Equation 1** application for calculating the SPF factor (290 nm-320 nm)[9,11] in accordance to the AuNPs amount. **Table 2** reports the SPF values at different AuNP concentration. At the increasing of SPF values, more effective is the product in preventing sunburn.[11] It is worth to mention that observing the AuNP UV-Vis spectrum (Figure 2A or **Figure S9** reporting the transmitted light by AuNPs), a great percentage of UV light was filtered and the effect, increasing the amount of AuNPs, appeared pronounced. The same approach was used by Salman *et al.*[51] obtaining a similar behavior: AuNPs deposited onto knitted fabrics, for biomedical purposes, increased the ultraviolet protection factor.[51]

Overall, Borase *et al.*[21] described that the most part of the used sunscreens shows UV-Vis spectra similar to that of AuNPs, corroborating our proposal to use the green-synthesized AuNPs as additional ingredient in cosmetic formulations for enhancing the SPF. In this context AuNPs can be considered as booster to increase the SPF in commercial formulation. Work in this direction is in progress in our laboratories. Moreover, due to the AuNP high absorption in the UVA spectral region, the protection against UVA light is also considered.

3.8. Antioxidant properties of AuNPs.

The evaluation of the total antioxidant capacity (TAC) or the TROLOX Equivalent Antioxidant Capacity (TEAC) may be considered a good tool for determining the antioxidant properties of various system, with particular application in food extract.[52] Among the various analytical methods for the evaluation of the antioxidant capacity, the DPPH method is very common.[53] $DPPH^{\bullet}$ is a stable free radical, thanks to the electron delocalization of the unpaired electron on the whole molecule, which determines also the occurrence of a purple color, with an absorption band around 520 nm. Indeed, if DPPH was completely reduced following the reaction reported in **Figure 6**, the solution color changes from purple to yellow.[22] Therefore, it is observed a bleaching of the absorption signal which linearly depends on the antioxidant concentration. TROLOX is used as reference antioxidant. In Figure 6, the DPPH absorption spectrum in the visible region was reported, showing a maximum at about 517 nm, diagnostic of the redox state.[22] As a first step, TROLOX was used as a positive control being able to efficiently reduce DPPH thanks to its antioxidant nature (Figure 6A).[22] Five TROLOX concentrations were used: 1.0×10^{-6} M, 1.0×10^{-5} M, 1.5×10^{-5} M, 2.0×10^{-5} M and 1.0×10^{-4} M. In particular, for TROLOX concentration below 1.0×10^{-6} M, only slight variations were observed in the DPPH visible spectrum, while increasing the concentrations, as reported in Figure 6A, incremental changes were observed. Interestingly, at 1.0×10^{-4} M TROLOX concentration, the absorption band at 517 nm completely disappeared. When AuNPs were taken into account, appreciable changes were detected at the concentration of 0.6×10^{-12} M. Further increasing concentration, the results reported in Figure 6B were observed.

After these considerations, **Equation 2** was used to infer the scavenging activity percentage both for TROLOX and for AuNPs in presence of DPPH.[22,40] **Figures S10** shows the obtained results.

Indeed, if **Equation 2** was applied for inferring the TAC, choosing as reference the amount of AuNPs or TROLOX able to scavenge the 10 % of DPPH, it is observed that TROLOX needs a higher concentration, i.e. 5.0×10^{-5} M (Figure S9A), in comparison with AuNPs (Figure S9B). Indeed, in the latter case, $2.0 \times 1\ 0^{-12}$ M appeared as the concentration able to scavenge the 10% of DPPH. Therefore, in order to obtain the same TAC, the TROLOX concentration has to be 2.5×10^{6} times greater than the concentration of AuNPs. Indeed the extract contains mixture of polyphenols that acts in synergy and also the concentration of the polyphenols in the extract thus around the AuNPs is higher than that of TROLOX. The pooling effect of phenols was thus observed.

This result indicated an extraordinary antioxidant capacity of this new typology of AuNPs, better confirmed by using biomolecules as primary acceptors of oxidant species. In particular, the AuNPs ability in the inhibition of the oxidative processes were evaluated in presence of H_2O_2, used as a ROS model.

3.9. Reaction between Cytochrome–c and H_2O_2.

As reported in literature, Cyt–c is a protein sensitive to the presence of H_2O_2 and the oxidative degradation affects its catalytic activity.[54] The process could be monitored observing the UV-Vis spectrum of the Cyt–c reported in **Figures S11**. Cyt–c presents an intense absorption band in the blue region of spectrum at 408 nm, usually indicated as Soret band, and a broad and not defined band around 535nm.[55] Both bands occurred affected by the presence of H_2O_2.[54,55] Overall the absorption spectrum of Cyt–c decreased its intensity during the H_2O_2-mediated oxidation indicating the protein degradation. 1.00×10^{-3} M of H_2O_2 was used a suitable concentration. Monitoring the absorption intensity at 408 nm (*A*), read at time *t*, normalized for the absorption value read at time zero (A_0), before the addition of H_2O_2, it was possible to obtain

information about the Cyt–c degradation in presence and in absence of AuNPs.[54,55] Different amount of AuNPs were used, in the range 1.80×10^{-12} M-1.00×10^{-11} M. **Figure S12** shows the obtained results and **Table S1** reports the percentage of Cyt–c degradation evaluated by using **Equation 3**, in absence and in presence of AuNPs at various reaction times. The reported data indicated that, increasing the NPs amount, the Cyt–c degradation percentage decreased. In other words, in presence of AuNPs the degradation of Cyt–c appeared delayed.

Beside these results, interestingly, in absence of H_2O_2, in Cyt–c solutions containing a low AuNP concentration, a fast and spontaneous protein reduction was observed (data not shown), with the appearance of the reduced Cyt−c characteristic band splitting in the UV-Vis spectrum, forming a new peak around 535 nm.[55] Overall, these results suggested the high antioxidant potential of phenol layer being able in reducing the Fe^{III} to Fe^{II}.[55]

3.10. Reaction between S^4TdR and H_2O_2.

The results obtained in presence of Cyt–c were unveiled using S^4TdR. In this condition, in order to better follow the molecule degradation in a reasonable time range, the H_2O_2 concentration was increased at 8.80×10^{-2} M. In our research group, S^4TdR was studied for several years.[24,25] The modified nucleoside is similar to its natural analogue, TdR, with a sulphur atom in position 4, which gives to the molecule an interesting reactivity towards ROS, making the molecule a chemical ROS probe.[24,25] In particular, when H_2O_2 was used as oxidant agent, S^4TdR was oxidized obtaining several products and, among them, the TdR and a hydroxylated reaction intermediate (R-SOH) were important. The former exhibited an absorption band in UV-Vis spectrum at around 265 nm, the latter at 360 nm. It is worth to mention, that the R-SOH hydrolysis induced the TdR formation.[56,57] The nature of these compounds was confirmed by a detailed molecular investigation by using ESI-MS and MS/MS at high

resolution (*data not shown*). Starting from these considerations, S^4TdR was used to test the antioxidant activity of AuNPs enabling the possibility to mimic a biological environment by using a modified nucleoside. The used AuNPs concentrations were 3.60×10^{-12} M and 1.00×10^{-11} M. The results are reported in **Figure S13**. Starting from the reaction conduced in absence of AuNPs (black line), after the first 5 minutes of reaction, a shoulder appeared around 360 nm, indicating the outcoming hydroxylated product R-SOH. If the AuNPs addition at 3.60×10^{-12} M induced slight spectral variations, on the other hand, further increasing the AuNP amount at 1.00×10^{-11}M, the nucleoside degradation occurred less pronounced with the shoulder around 360 nm less evident than the previous case. These results indicated the protective role of AuNPs. The scenario became more interesting after 60 minutes of reaction. As already mentioned, the TdR formation is related to the R-SOH hydrolysis, thus the R-SOH degradation (at 360 nm) induces the formation of the band at 265 nm as reported in Figures S13. When AuNPs were added in the mixture, the band at 360 nm was more evident, if compared with the scenario observed in absence of AuNPs. Indeed, AuNPs, preserving the S^4TdR oxidation, retarded the R-SOH formation affecting in turn the TdR production. The band at 265 nm was in fact not pronounced. Moreover, the detailed analysis of the UV-Vis spectra reveals that, increasing the AuNPs concentration (after 60 minutes, green line), the expected R-SOH band at 360 nm was instead located at 358 nm, due to the S^4TdR contribute at 337 nm.

3.11. Cytoxicity of AuNPs.

A sufficient intracellular AuNP uptake, not compromising the viability, is an important parameter in assessing whether a nanomaterial can be used for *in vivo* tests. Hence, we examined the incremental dose uptake profile, along with a cytotoxic assay. In essence, Human Microvascular Endothelial Cells (HMVEC) and Human Dermal Fibroblasts (HDF) were

incubated with increasing doses of AuNPs for 72h and measurements of cell viability were conducted using trypan blue assay, as described in the Experimental Section. As shown in **Figure 7** AuNPs did not exert any obvious cytoxicity within the concentrations 1.80×10^{-12} M-3.60×10^{-12} M for both cell lines, whereas in cultures treated with the maximum dose (1.00×10^{11} M) the viability significantly decreased to levels below the starting plating density for HMVEC (1.0×10^{5} cells) and remained to the seeding number for HDF. Morphologic examination (with a conventional optical microscope under white light illumination) of HMVEC and HDF exposed to increasing AuNP concentration (from 1.80×10^{-12} M to 1.00×10^{-11} M), after May-Grunwald Giemsa staining, demonstrated the dose-dependent cellular uptake. The internalized metal loads are identified as the black areas inside the cells and the captured images confirmed the cytotoxic effect of the highest concentration of gold in both cell lines. Therefore we believe that the use of AuNPs within 3.60×10^{-12} M is safe and feasible.

3.12. Effects of AuNPs on biological cell feature of HMVEC

Branching morphogenesis is a complex developmental program that regulates the formation of the vascular system. To assess the ability of endothelial cells to differentiate into capillary-like networks, cells are overlaid with a thin layer of Matrigel and in which migrate to form a complex network of structures resemble capillaries in that they are multicellular and contain lumens.

To assess possible effects of AuNPs on biological or functional cell activities, vehicle and AuNP treated HMVEC were induced to capillary morphogenesis. As shown in **Figure 8**, HMVEC loaded with the two safe doses of AuNP were able to form interconnecting network of capillary tubes with the same effectiveness as vehicle treated cells, and the degree of differentiation was then quantified as number of closed meshes. These results not only show

that AuNP heavily loaded HMVEC preserved their ability to differentiate in tubular-like structures, but also that AuNPs are retained inside the cells after having been induced to differentiate.

4. Conclusions

The scientific interest for the use of AuNPs is well described by Qin *et al*. [59] in their recent review in which present the AuNPs as versatile nanomaterials. In particular in this paper, the green synthesis of AuNPs using the PGJ is presented as an inexpensive approach with great advantages if compared with similar papers [18,19]. The obtained AuNPs are presented as booster in cosmetic formulations to enhance the antioxidant behavior and the SPF values. Thanks to the mild reaction condition necessary for controlling the nanostructured particle formation, a great improvement is obtained in this field. [15] Indeed, the plant-based synthesis of AuNPs is gaining importance due to its low cost, biocompatibility and eco-friendliness.[15,16] In this work, the AuNPs formation was confirmed by UV-Vis and FTIR spectroscopies, and XPS analysis, evidencing the typical characteristic signals of PGJ phenolic component. AuNPs were obtained in a reasonable time range, at least 4h, using an appropriate amount of $HAuCl_4$. The acid pH value of the juice (pH 3) resulted to be the optimal condition for the synthesis. Indeed, at pH values greater than 3 (during the synthesis), aggregated AuNPs were obtained. The observed well defined shape of the surface plasmon resonance band at 577 nm, typical of AuNPs, suggested that, in our experimental conditions, uniformly distributed and not aggregated NPs, with a diameter of about 100 ± 40nm, were obtained in water solution. SEM images better proved these results, showing AuNPs with irregular domains. TEM images further confirmed this finding, evidencing also the presence of a 6nm wide organic layer surrounding AuNPs. The synthesized AuNPs were stable in time and under extreme conditions of pH values and temperatures. Only at pH 2, the aggregation of AuNPs was observed. The

measured Zeta Potential changed from negative values of -22 mV, in the region of pH values 4-12, to positive ones at pH 2, justifying the NP aggregation. Moreover, the obtained AuNPs, thanks to the presence of phenolic organic layer onto their surface, showed a significant antioxidant behavior, together with the additional property of screening the sun radiation. The antioxidant property was investigated also monitoring the oxidation of suitable H_2O_2-mediated probes at different time. In particular, S^4TdR and Cyt–c were used for mimicking the presence of biological molecules. The inhibition of their degradation was observed in absence and in presence of different AuNPs concentrations. The AuNPs photostability under sun irradiation, together with the high absorption in the UV-Vis range, open the possibility of using the particles as an efficient skin protector from UV light. Indeed, the high absorbance of the phenolic organic layer present around AuNPs in this spectral region, makes them possible candidates to enhance the SPF in sunscreen formulations. The calculated SPF values were in the range from 3 to 18 and were obtained in relation to the amount of AuNPs. The SPF should be increased, increasing the amount of AuNPs. However, the nanotoxicological studies carried out by using dermal fibroblasts (to evaluate the possible detrimental effects of these nanoparticles) and endothelial cells (as a relevant model since they lining the lumen of all blood vessels they serve as first contact with NPs) indicated that an AuNP concentrations in the range 1.80×10^{-12} M - 3.60×10^{-12} M should be adopted in order to be not cyctotoxic. As a results, the possibility to use antioxidant AuNPs as booster in possible sunscreen formulations exhibiting an SPF value of 6 is thus presented and the findings would form a possible future platform for designing PGJ-based nano-structured systems, with improved properties, for cosmetic applications, preventing also the UV-induced ROS production.

Acknowledgements

We gratefully acknowledge Mr. Sergio Nuzzo for the skillful and excellent technical assistance and for the camera pictures reported in Figure 1. We thanks Mr. Adriano Boghetich for the SEM images acquisition and his precious collaboration. This work was supported by the financial support of the Italian Ministry for Education, University and Research (MIUR) under grant PONa3_00369 and of the project "NANOAPULIA – NANO fotocatalizzatori per un'atmosfera più pulita" (CUP: B38C14000510008).

References

[1] D.M.J. Houston, B. Robins, J.J. Bugert, S.P. Denyer, C.M. Heard, *European Journal of Pharmaceutical Sciences* **2017**, *96*, 99

[2] Z. Kalaycıoglu, F. B. Erim. *Food Chemistry* **2017**, *221*, 496

[3] Y. Noda, T.Kaneyuki, A.Mori, L.Packer. *J. Agric. Food Chem.* **2002**, *50*, 166

[4] D.N. Syed, J-C Chamcheu, V. M. Adhami, H. Mukhtar. *Anticancer Agents Med Chem.* **2013**, *13(8)*, 1149.

[5] P. Sharma, S. F. Mc Clees, F. Afaq. *Molecules* **2017**, *22*, 177.

[6] S. Medhe, P. Bansal, M.M. Srivastava. *Appl. Nanosci.* **2014**, *4*, 153.

[7] M. Yoshimura, Y. Watanabe, K. Kasai, J. Yamakoshi, T.Koga. *Biosci. Biotechnol. Biochem.* 2005, **69(12)**, 2368–2373

[8] M.C.L. Marchiori, C. Rigon, C. Camponogara, S.M. Oliveira, L. Cruz. *J Photoch Photobio B* **2017**, *170*, 25.

[9] L. Mbanga, M. Mulenga, P.T. Mpiana, K. Bokolo, M. Mumbwa, K. Mvingu, *International Journal of Advanced Research in Chemical Science* **2014**, *1(8)*, 7.

[10] L.R. Sklar, F. Almutawa, H.W. Lim, I. Hamzavi. *Photochem. Photobiol. Sci.* **2013**, *12*, 54.

[11] E.A. Dutra, D.A. Gonçalves da Costa e Oliveira, E.R.M. Kedor- Hackmann, M.I.R.M. Santoro. *Braz J Pharm Sci.* **2004**, *40(3)*, 381.

[12] D.I.M. Amararatne, W.A.P. Weerakkody, J.A.L.P. Jayakody. *Trop Agr Res*. **2012**, *23(4)*, 370.

[13] D. Xian, X. Gao, X. Xiong, J. Xu, L. Yang, L. Pan, J. Zhong. *J Photoch Photobio B* **2017**, *175*, 73

[14] L. Qin , G. Zeng, C. Lai, D. Huang, C. Zhang, P. Xu, T. Hu, X. Liu, M. Cheng, Y. Liu, L. Hu, Y. Zhou, *Sensors & Actuators: B. Chemical*, **2017**, 243, 946.

[15] S.S. Dash, B.G. Bag. *Appl Nanosci*. **2014**, *4*, 55.

[16] A.M. Abdelmonema, R.M. Amin. *Int. J. Sci.: Basic, Applied Research* **2014**, *15(1)*, 57.

[17] A. Chakraborty, N. R. Jana. *ACS Applied Materials and Interfaces*, **2017**, 9(48), 41807

[18] V. Sanna , N. Pala, G. Dessì, P. Manconi, A. Mariani, S. Dedola, M. Rassu, C. Crosio , C. Iaccarino, M. Sechi. *Int. J. Nanomedicine*, **2014**, 9, 4935.

[19] H. Dar-Shih , L. Hsiu-Chin, C. Cheng-Cheung, W. Chang-Jer , Y. Ming-Kung. *Int. J. Nanomedicine*, **2012**, 7, 1623.

[20] Z.E. Jiménez-Pérez, P. Singh, Y.-J. Kim, R. Mathiyalagan, D.-H. Kim, M.H. Lee, D.C. Yang. *J Ginseng Res* **2017**, 1

[21] H.P. Borase, C.D. Patil, R.B. Salunkhe, R.K. Suryawanshi, B.K. Salunke, S.V. Patil. *J. Cosmet. Sci.* **2014**, *36*, 571.

[22] S.B. Kedare, R.P. Singh. *J Food Sci Technol.* **2011**, *48(4)*, 412.

[23] H. Swalwell, J. Latimer, R.M. Haywood, M.A. Birch-Machin. *Free Radical Bio Med.* **2012**, *52*, 626.

[24] V. Rizzi, I. Losito, A. Ventrella, P. Fini, A. Agostiano, F. Longobardi, P. Cosma. *RSC Advances* **2014**, *4*, 48804.

[25] V. Rizzi, I. Losito, A. Ventrella, P. Fini, A. Fraix, S. Sortino, A. Agostiano, F. Longobardi, P. Cosma. *Phys. Chem. Chem. Phys*. **2015**, *17*, 26307.

[26] V.Rizzi, P. Fini, F. Fanelli, T. Placido, P. Semeraro, T. Sibillano, A. Fraix, S. Sortino, A. Agostiano, C. Giannini, P. Cosma. *Food Hydrocolloid* **2016**, *58*, 98.

[27] M. Hüttemann, P. Pecina, M. Rainbolt, T.H. Sanderson, V.E. Kagan, L. Samavati, J.W. Doan, I. Lee. *Mitochondrion* **2011**, *11(3)*, 369.

[28] A.M. Alkilany, C.J. Murphy. *J Nanopart Res.* **2010**, *12(7)*, 2313.

[29] C.J. Murphy, A.M. Gole, J.W. Stone, P.N. Sisco, A.M. Alkilany, E.C. Goldsmith, S.C. Baxter, *Acc Chem Res.* **2008**, *41(12)*,1721.

[30] C.M. Goodman, C.D. McCusker, T. Yilmaz, V.M. Rotello, *Bioconjug Chem.* **2004**, *15(4)*, 897.

[31] E.E. Connor, J. Mwamuka, A. Gole, C.J. Murphy, M.D. Wyatt. *Small*. **2005**, *1(3)*, 325.

[32] N. Lewinski, V. Colvin, R. Drezek *Small*. **2008**, *4(1)*, 26.

[33] Y. Cao, Y. Gong, L. Liu, Y. Zhou, X. Fang, C. Zhang, Y. Li, J. Li *J Appl Toxicol.* **2017**, *37(12)*, 1359.

[34] C. Freese, L. Anspach, R.C. Deller, S.J. Richards, M.I. Gibson, C.J. Kirkpatrick, *Biomater Sci.* **2017**, *285(4)*, 707.

[35] K. Esumi, N.Takei, T. Yoshimura. *Colloids, Surfaces B* **2003**, *32*, 117.

[36] Á.I. López-Lorente, M. Valcárcel, B. Mizaikoff. *Microchim Acta* **2014**, *181*, 1101.

[37] C.A. Pedriali, A.U Fernandes, P.A. dos Santos, M.M. da Silva, D. Saverino, M.B. da Silva *Ciênc. Tecnol. Aliment.* **2010**, *30(4)*, 1017.

[38] M.I. Gil, F.A. Tomas-Barberan, B. Hess-Pierce, D.M. Holcroft, A.A. Kader, *J. Agric. Food Chem.* **2000**, *48*, 4581.

[39] N. Ahmad, S. Sharma, R. Rai. *Adv. Mat. Lett.* **2012**, *3(5)*, 376.

[40] S. Sreekumar, H. Sithul, P. Muraleedharan, J.M. Azeez, S. Sreeharshan, *Bio Med Res Int* **2014**, 1-12

[41] A. Zarfeshany, S. Asgary, S.H. Javanmard. *Adv Biomed Res.* **2014**, *3(1)*, 100.

[42] M. Goudarzi, N. Mir, M. Mousavi-Kamazani, S. Bagheri, M Salavati-Niasari. *Scientific Reports*. **2016**, *56*, 32539.

[43] Y. Tan, Y. Li, D. Zhu. *Langmuir* **2002**, *18*, 3392.

[44] X. Li, Y. Li, Y. Tan, C. Yang, Y. Li. J. Phys. Chem. B. **2004**, *108*, 5192.

[45] C.S. Love, V. Chechik, D.K. Smith, K. Wilson, I. Ashworth, C. Brennan. *Chem. Commun.* **2005**, *15*, 1971

[46] P. Jiang, J.-J. Zhou, R. Li, Z.-L. Wang, S.-S. Xie, *Nanotechnology* **2006**, *17*, 3533.

[47] J. Xie, J.Y. Lee, D.I.C. Wang, *J. Phys. Chem. C.* **2007**, *111*, 10226.

[48] M.P. Casaletto, A. Longo, A. Martorana, A. Prestianni, A.M. Venezia, *Surf. Interface Anal.* **2006**, *38*, 215.

[49] V. Laquintana, N. Denora, A. Lopalco, A. Lopedota, A Cutrignelli, F.M. Lasorsa, G. Agostino, M. Franco. *Mol. Pharm.* **2014**, *11*, 859.

[50] C.D. Kaur, S. Saraf. *Pharmacognosy Res.* **2010**, *2(1)*, 22.

[51] A.A. Salman, H.M. Ibrahim, K.M. Hassan, A.A. Hussen, S.M. Abuelhassan. *Der Pharma Chemica*, **2017**, *9(7)*, 13.

[52] A.M. Pisoschi, G.P. Negulescu. *Biochem & Anal Biochem* **2011**, *1*, 106.

[53] E.J. Garcia, T.L.C. Oldoni, S.M. de Alencar, A. Reis, A.D. Loguercio, R. *Braz Dent J* **2012**, *23(1)*, 22.

[54] J.A. Villegas, A.G. Mauk, R. Vazquez-Duhalt, *Chemistry & Biology*. **2000**, *7*, 237.

[55] V. Rizzi, P. Fini, P. Semeraro, P. Cosma. *Colloids, Surfaces B* **2016**, *142*, 239.

[56] N. Ramnath, V. Ramesch, V.J.C.S. Ramamurthy, *J. Chem. Soc., Chem. Commun.* **1981**, *0*, 112.

[57] V. Ramesch, N. Ramnath, V. Jayathertha Rao, V. Ramamurthy. *J. Photochem.* **1982**, *18*, 109.

[58] A. Laurenzana, F. Cencetti, S. Serratì, G. Bruno, L. Japtok, F. Bianchini, E. Torre, G. Fibbi, M. Del Rosso, P. Bruni, C. Donati. *J. Mol. Med.* **2015**, *93*, 1145.

[59] L. Qin, G. Zeng, C. Lai, D. Huang, P. Xu, C. Zhang, M. Cheng, X. Liu, S. Liu, B. Li, H. Yi. *Coordination Chemistry Reviews*, **2018**, 359, 1.

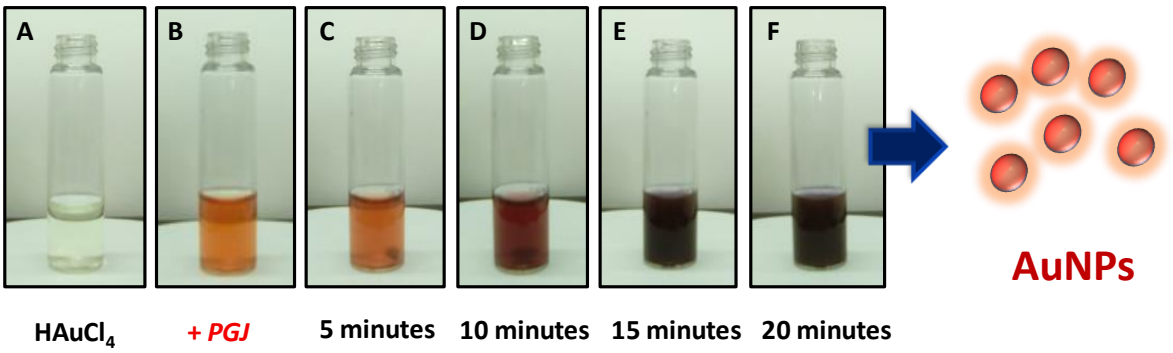

Figure 1. Camera pictures of solutions containing 1.5mL of $HAuCl_4$ 1 mM, 2.0 mL of water before (A) and after (B) the addition of PGJ (500 μL). Pictures from (C) to (D) are related to the time evolution of AuNPs formation after the PGJ addition. The mixture was moderately stirrer at room temperature.

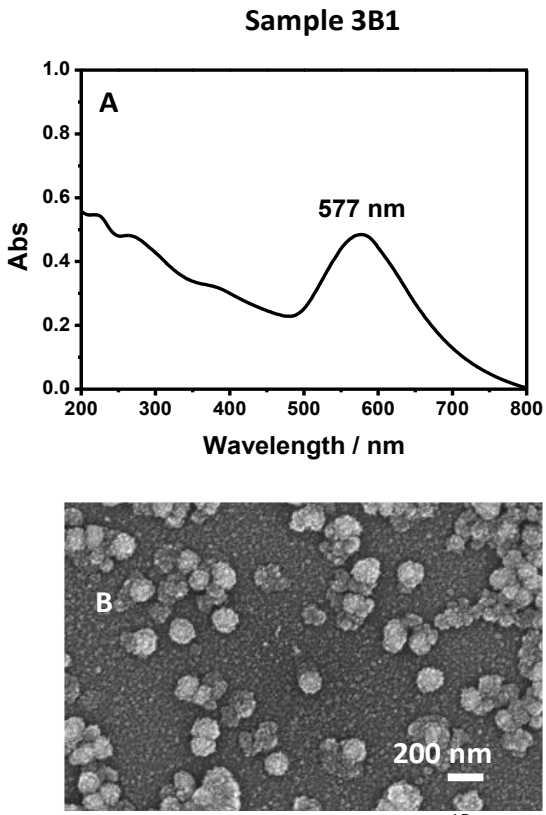

Figure 2. UV-Vis absorption spectrum of AuNPs (3.60×10^{-12} M) in water obtained using the condition 3B1 reported in Table 1 (A) and the related SEM image (B). The AuNPs after the synthesis were repeatedly washed with water.

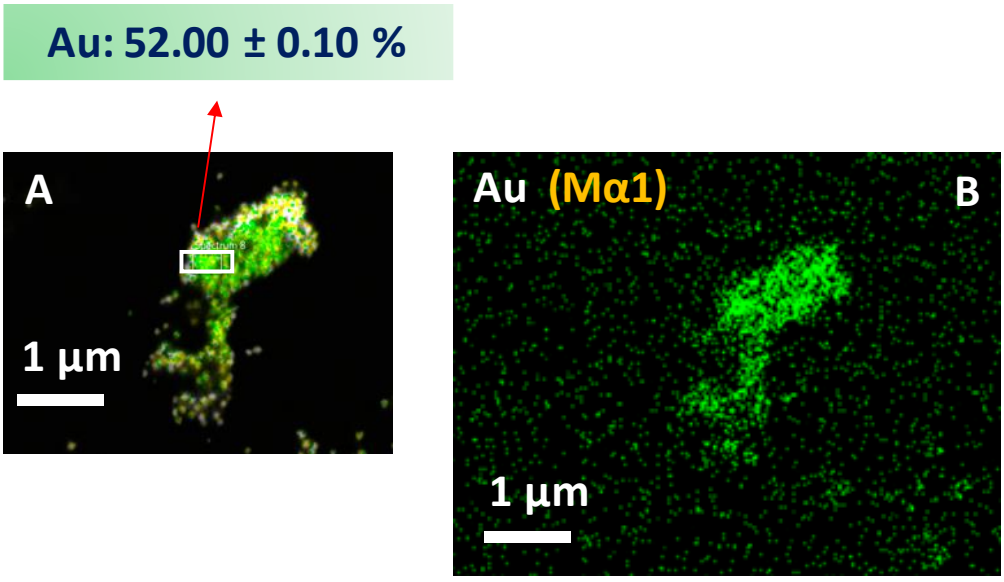

Figure 3. EDX analysis of AuNPs. The areas analyzed by EDX are marked by different colors: green for the Au detection and yellow for Carbon, mostly derived from the graphite used during the sputtering process. In detail, the image **A** (In-Lens SEM) reports an area in which an high number of aggregated AuNPs were collected with the evident chemical composition reported in picture **B** as a map. The area evidenced in picture **A** (white rectangle) indicates that in this region the Au was the 52.00 ± 0.10 % of the total chemical composition.

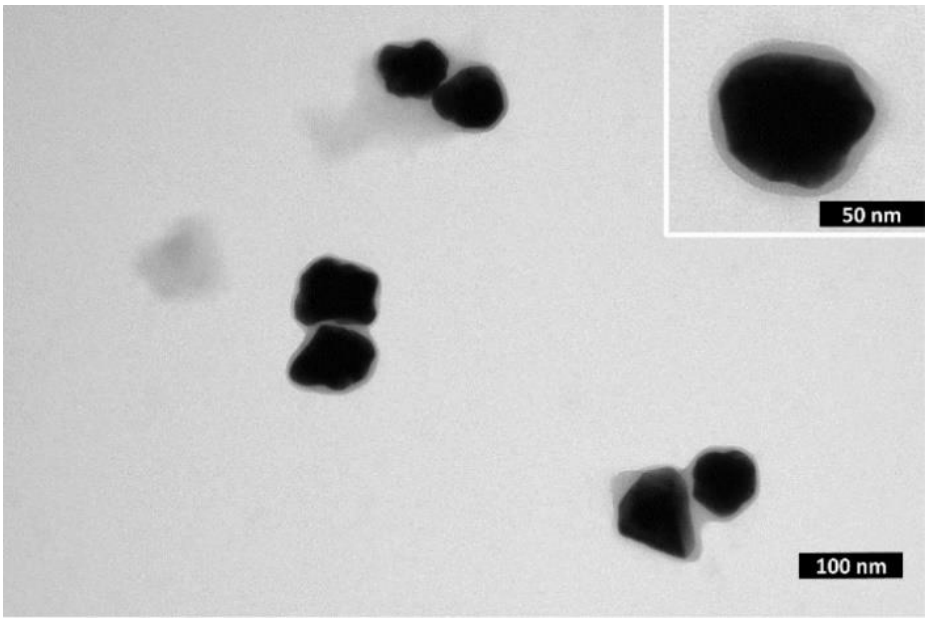

Figure 4. TEM micrographs of AuNPs. The inset shows a detail of a single Au NPs surrounded by a continuous organic coating evidenced by the light grey layer around the NPs.

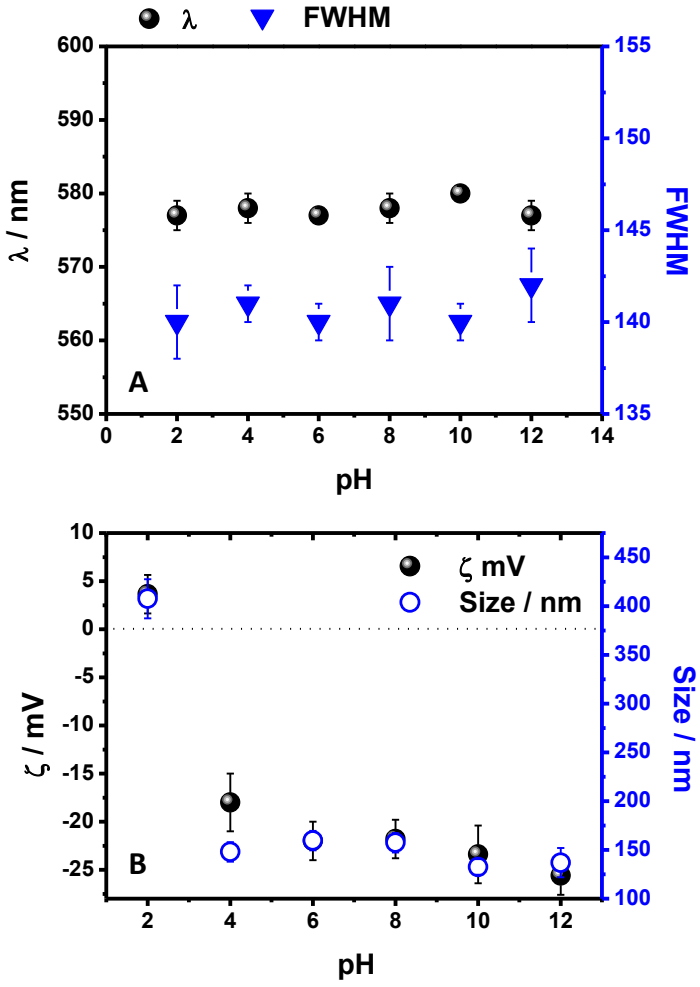

Figure 5. Time stability of AuNPs having a concentration 3.60 × 10^{-12} M at different pH values ranging from 2 to 12 (**A**). The wavelength (λ) read at 577 nm and the FWHM in function of the pH are reported. The Zeta potential and AuNPs size were measured in the same pH range (**B**).

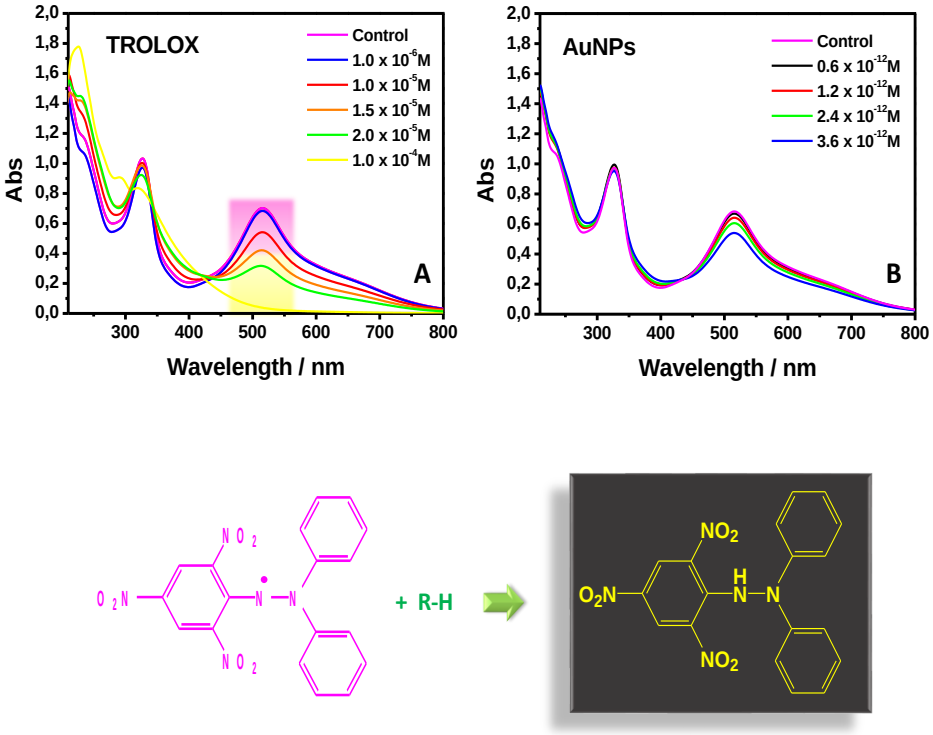

Figure 6. Absorption spectra of DPPH in presence of TROLOX (**A**) and AuNPs (**B**) at different concentrations.

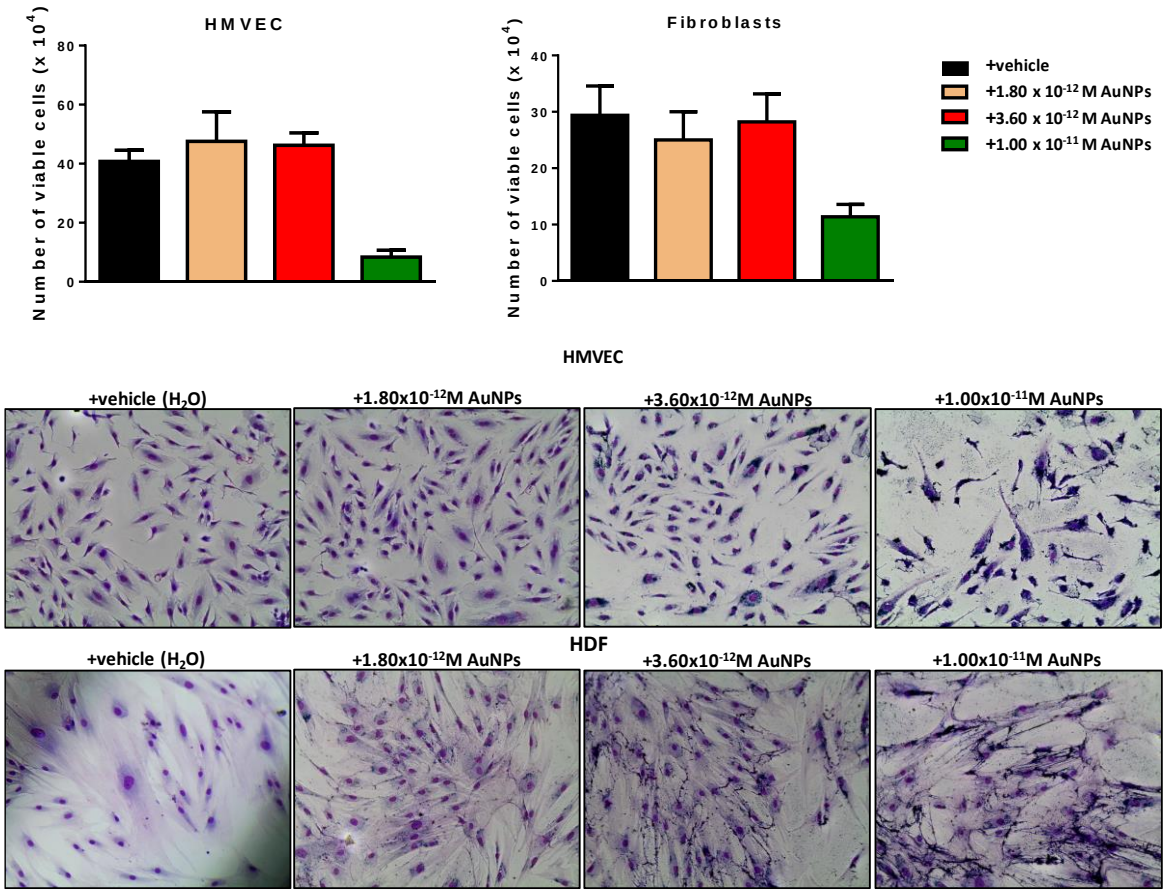

Figure 7. Cytotoxicity of AuNPs after 72 h exposure on HMVEC and HDF: on the upper panel, histogram representing viable cells (trypan blue negative) counted with the aid of a Burker chamber, as described in Experimental Section. On the bottom, images of May-Grunwald Giemsa stained cells acquired using phase contrast microscopy confirmed the effective endocytosis of AuNPs at increasing concentrations of Au in the incubation solution. The inner gold content is represented by the black dots in the cells.

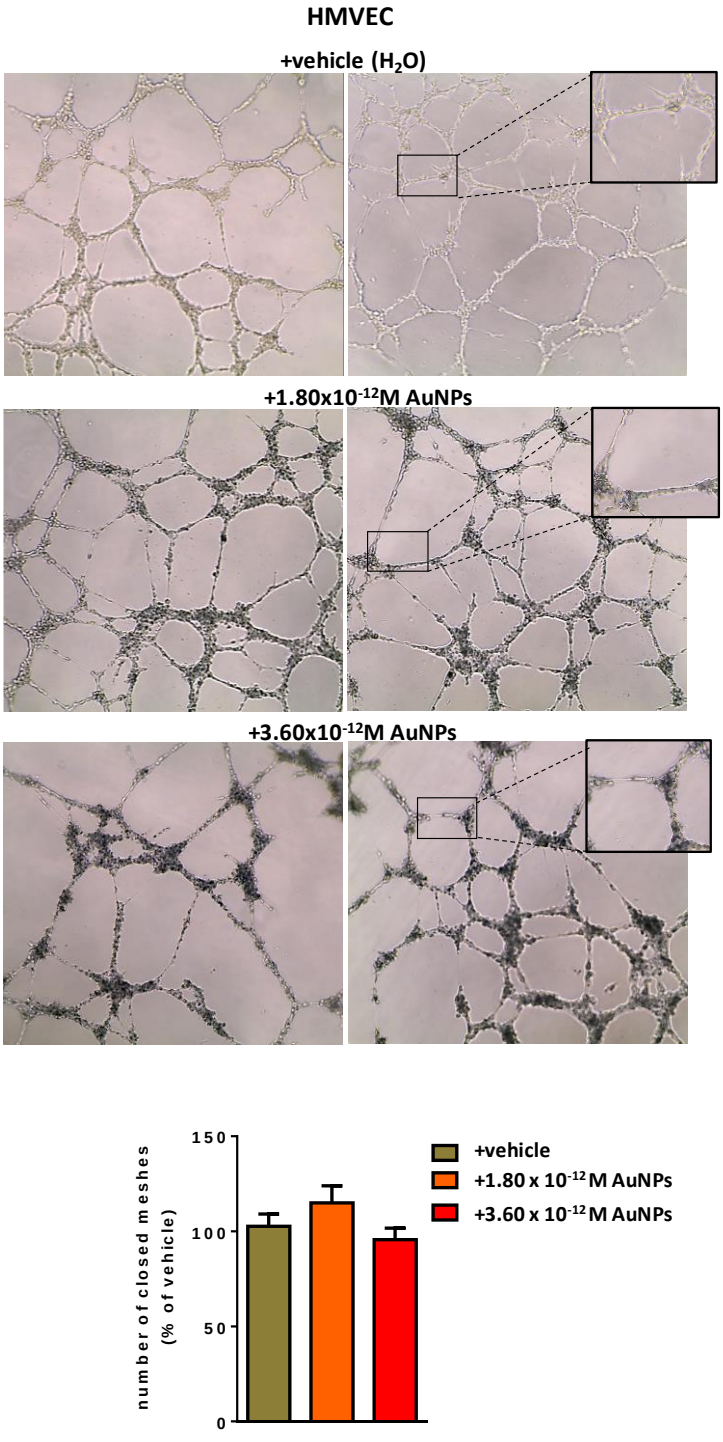

Figure 8. Representative visualization of tubulogenesis assay after pre-treatment of HMEC cells with vehicle or with the not toxic doses of AuNPs (1.80×10^{-12} M, 3.60×10^{-12} M) for 48h. Cells were then cultured on Matrigel matrix supports. Cell organization was examined microscopically (a detailed enlarged structure is shown in the inset) taking random photomicrographs after 6h with the aid of a Nikon E 4500 photo camera (Nikon) on a Nikon

TMS-F phase contrast microscope (Nikon Instruments) and quantified by manually counting the number of closed meshes/field reported as percent of the vehicle

Sample	$C_{Au\ III}$ (M)	$V_{Au\ III}$ µL	V_{H2O} µL	V_B pH 7 µL	V_B pH 12 µL	V_E µL	$\frac{V_{Au}}{V_E}$	[AuNPs]
1	1.50×10^{-4}	1500 (from 2×10^{-4} M)	//	//	//	500	3 : 1	**n.d**
2	5.00×10^{-4}	1000 (from 1×10^{-3} M)	//	//	//	1000	1 : 1	**n.d**
3A	1.90×10^{-4}	1500 (from 1×10^{-3} M)	4000	//	//	500	3 : 1	**1.0×10^{-11}M**
3B1	3.75×10^{-4}	1500 (from 1×10^{-3} M)	2000	//	//	500	3 : 1	**2.0×10^{-11}M**
3B2	3.75×10^{-4}	1500 (from 1×10^{-3} M)	//	2000	//	500	3 : 1	**aggregated and irregular**
3B3	3.75×10^{-4}	1500 (from 1×10^{-3} M)	//	//	2000	500	3 : 1	**aggregated and irregular**
3C	7.50×10^{-4}	1500 (from 1×10^{-3} M)	//	//	//	500	3 : 1	**slightly aggregated and not uniform**
4A	1.75×10^{-4}	1750 (from 1×10^{-3} M)	8000	//	//	250	7 : 1	**Not uniform in the shape: presence of rods**
4B	2.20×10^{-4}	1.750 (from 1×10^{-3} M)	6000	//	//	250	7 : 1	**Not uniform in the shape: presence of rods**
4C	2.90×10^{-4}	1750 (from 1×10^{-3} M)	4000	//	//	250	7 : 1	**Not uniform in the shape: presence of rods**
4D1	4.38×10^{-4}	1750 (from 1×10^{-3} M)	2000	//	//	250	7 : 1	**Not uniform in the shape: presence of rods**
4D2	4.38×10^{-4}	1750 (from 1×10^{-3} M)	//	2000	//	250	7 : 1	**aggregated and irregular**
4D3	4.38×10^{-4}	1750 (from 1×10^{-3} M)	//	//	2000	250	7 : 1	**aggregated and irregular**
4E	8.75×10^{-4}	1750 (from 1×10^{-3} M)	//	//	//	250	7 : 1	**Not uniform in the shape: presence of rods**
5	5.00×10^{-3}	1000 (from 1×10^{-2} M)	//	//	//	1000	1 : 1	**aggregated and irregular**
6	6.25×10^{-3}	1250 (from 1×10^{-2} M)	//	//	//	750	1.6:1	**aggregated and irregular**
7A	2.50×10^{-3}	1500 (from 1×10^{-2} M)	4000	//	//	500	3 : 1	**aggregated and irregular**
7B1	3.75×10^{-3}	1500 (from 1×10^{-2} M)	2000	//	//	500	3 : 1	**aggregated and irregular**
7B2	3.75×10^{-3}	1500 (from1×10^{-2} M)	//	2000	//	500	3 : 1	**aggregated and irregular**
7B3	3.75×10^{-3}	1500 (from 1×10^{-2} M)	//	//	2000	500	3 : 1	**aggregated and irregular**
7C	7.50×10^{-3}	1500 (from1×10^{-2} M)	//	//	//	500	3 : 1	**aggregated and irregular**
8	8.75×10^{-3}	1750 (from 1×10^{-2} M)	//	//	//	250	7 : 1	**aggregated and irregular**

Table 1: Conditions of work adopted during the synthesis of AuNPs. $C_{Au\ III}$, $V_{Au\ III}$, V_{H2O}, V_B and V_E represent the final concentrations of $HAuCl_4$, the volume of added $HAuCl_4$, the volume of added water/buffer and the volume of extract in the mixture. V_{Au}/V_E represents the ratio between the volume of $HAuCl_4$ and PGJ. Legend: n.d = not detected

Table 2. SPF calculated in the range 290-320nm calculated using Equation 1. The SPF values are referred to solutions containing different AuNPs concentrations

AuNPs [$\times 10^{-12}$M]	1.80	3.60	7.20	10.0
SPF (290-320nm)	3	6	12	18